Chapter 7
Riboflavin-Conjugated Multivalent Dendrimer Platform for Cancer-Targeted Drug and Gene Delivery

Pamela T. Wong, Kumar Sinniah and Seok Ki Choi

Abstract Riboflavin receptors (RFRs) are overexpressed in several malignant cells, and have been characterized as an emerging tumor surface biomarker. In this article, we discuss the design principles of a RFR-targeted nanoparticle system and illustrate its applications with studies performed in our laboratories. This system is based on a poly(amidoamine) (PAMAM) dendritic polymer which is modified on the surface by conjugation with riboflavin (RF) as the targeting ligand. First, we discuss the application of this system for targeted drug delivery by its conjugation with methotrexate as an antitumor payload. In cell-based experiments performed in vitro, this drug conjugate displayed RF-dependent, potent inhibition of cell growth in RFR(+) KB carcinoma cells. Second, the use of the RF-conjugated dendrimer for gene delivery applications through the formation of polyplexes with plasmid DNA is described. The ability of this targeted system to significantly enhance gene transfection in epithelial cells points to its potential as a promising new class of nonviral vectors. Third, the tunability of the functional properties of the dendrimer through modular integration is illustrated with an optically active gold nanoparticle (AuNP). The resultant dendrimer-coated AuNPs have a unique capability for tumor cell imaging via surface plasmon resonance scattering. Finally, we discuss the biophysical basis of the multivalent mechanism involved in the tight and specific binding of a RF-conjugated multivalent dendrimer to RFRs on the cell surface. The design principles and proof of concept studies presented here are

P.T. Wong (✉) · S.K. Choi (✉)
Michigan Nanotechnology Institute for Medicine and Biological Sciences,
and Department of Internal Medicine, University of Michigan Medical School,
Ann Arbor, MI 48109, USA
e-mail: ptw@med.umich.edu

S.K. Choi
e-mail: skchoi@med.umich.edu

K. Sinniah (✉)
Department of Chemistry and Biochemistry, Calvin College,
3201 Burton St. SE, Grand Rapids, MI 49546, USA
e-mail: ksinniah@calvin.edu

B. Yan et al. (eds.), *Bioactivity of Engineered Nanoparticles*,
Nanomedicine and Nanotoxicology, DOI 10.1007/978-981-10-5864-6_7

strongly supportive of the promising potential of RF-conjugated nanoparticles for delivery and imaging applications in tumors.

Keywords Riboflavin · Tumor surface marker · PAMAM dendrimer · Targeted delivery · Multivalent avidity · Surface plasmon resonance · Imaging cavity

Abbreviations

AFM	Atomic force microscopy
BSA	Bovine serum albumin
DAPP	3,8-Diamino-6-phenylphenanthridinium
DLS	Dynamic light scattering
EPR	Enhanced permeation and retention
EGFR	Epidermal growth factor receptor
FGFR	Fibroblast growth factor receptor
FAD	Flavin adenine dinucleotide
FMN	Flavin mononucleotide
FITC	Fluorescein isothiocyanate
FAR	Folate receptor
G5	Generation 5
AuNP	Gold nanoparticle
HPMA	*N*-(2-hydroxypropyl)methacrylamide
ITC	Isothermal titration calorimetry
MTX	Methotrexate
NP	Nanoparticle
pDNA	Plasmid DNA
PAMAM	Poly(amidoamine)
PSMA	Prostate-specific membrane antigen
RF	Riboflavin
RFBP	Riboflavin binding protein
RFR	Riboflavin receptor
SPR	Surface plasmon resonance

7.1 Introduction

Identification of tumor-associated surface markers plays a fundamental role in the design strategy for tumor-targeted nanoparticles (NPs) [1]. NP conjugation with a ligand molecule of high specificity for the particular biomarker of interest constitutes the basis for the mechanism of active tumor targeting [2, 3]. Optimal ligand conjugation design confers these NPs with a greater ability to facilitate tumor-specific NP binding and payload uptake than passive targeting mechanisms which rely solely on the enhanced permeation and retention (EPR) effect in which NPs accumulate in the tumor through the enhanced leakiness of tumor vasculature [4].

Several classes of tumor biomarkers have already been identified and used in the development of targeted NPs [1–3, 5]. These include: (1) receptors for vitamin uptake such as the folate receptor α, β (FAR_{α}, FAR_{β}) [6, 7], biotin receptor [8, 9]; (2) an integrin family of receptors such as $\alpha_v\beta_3$ [10]; (3) prostate-specific membrane antigen (PSMA) receptor [11, 12]; (4) growth factor receptors including HER2 [13], epidermal growth factor receptor (EGFR) [14], fibroblast growth factor receptor (FGFR) [15]; insulin receptors [16]; and (5) the transferrin receptor [17]. Each of these tumor biomarkers is overexpressed in one or more types of tumors and engages in receptor-mediated endocytosis [18], which serves as the specific route for the internalization of targeted NPs.

Riboflavin receptors (RFRs) belong to the class of vitamin uptake receptors which show promising potential for tumor-targeted applications [19, 20]. In an earlier study, Low et al. [21] investigated the cellular uptake mechanism of riboflavin (RF)-conjugated bovine serum albumin (BSA) in several human tumor cell lines. Uptake of this conjugate occurred at a rate greater than that of unmodified BSA, and the process was RFR-dependent and specific. Such facilitated protein uptake was attributed to RFR-mediated endocytosis, and highlighted the potential of using a RFR-targeted strategy for enhancing specific delivery. A research group led by Swaan, P.W. later also demonstrated the receptor-mediated uptake of a RF-rhodamine dye conjugated form [22, 23] in human cell lines.

Recently, we [24–28] and others [29–32] have started the development of RFR-targeted delivery platforms, and have conducted several proofs of concept studies in vitro and in vivo for their validation in tumor-targeted delivery. In this review article, we aim to describe our approaches in the design of RF-conjugated NPs, and provide several lines of evidence supportive of their significance and potential as a novel platform for tumor-targeted delivery. The purpose of this chapter is primarily to address the current lack of reviews and perspectives focused on RFR-targeted applications. Other established tumor biomarkers such as FARs [33, 34], integrin $\alpha_v\beta_3$ [10], PSMA receptor [35], HER2 [13, 36], and EGFR [14, 37] are already extensively reviewed elsewhere and thus are introduced only minimally here. We believe that this review provides a timely coverage of the various aspects important to RFR-targeted drug and gene delivery, and will serve as an invaluable resource in the design of RFR-targeted nanoplatforms.

7.2 Riboflavin Receptors and Ligands

In cellular metabolism, RF (vitamin B2) is required in the biosynthesis of flavin-based redox cofactors including flavin mononucleotide (FMN) and flavin adenine dinucleotide (FAD). However, its hydrophilicity ($\log P = -1.46$; P = partition coefficient = $[RF]_{octanol}/[RF]_{water}$) makes it unable to passively diffuse across hydrophobic cell membranes [38]. Thus, its cellular availability depends on the uptake mechanism mediated by its receptors.

Table 7.1 Properties of riboflavin receptors (RFRs)

Isoform	Biochemistry [40, 41]	Ligand	Tissue distribution
Soluble: riboflavin binding/carrier protein [45] Membrane-bound: riboflavin uptake transporter [23, 39, 40]	Glycosylated 219–469 Amino acids 27.5–40 kD_a	RF [41] Lumiflavin, Roseoflavin [47] Quinacrine [25]	Placenta [40], Small intestine [40], Breast [19, 39], Prostate [20], Liver [17], Cancer stem cells [43]

7.2.1 RFRs

A group of multiple proteins is involved in the cellular uptake of RF, consisting of RF carrier, RF transporter, and RF binding protein (RFBP). In this article, these proteins are collectively referred to as riboflavin receptors (RFRs) (Table 7.1). They are expressed as both soluble and membrane-bound isoforms [23, 39–41], and are involved primarily in cellular trafficking and uptake of RF. RFRs display high RF affinity as illustrated by RFBP ($K_D \approx 1$ nM) [41]. Recent studies suggest that RFRs are overexpressed in certain malignant cells including human breast and prostate tumors, which implicate RFRs as a class of tumor biomarkers [19, 20, 32]. Thus, these cells displayed the unique ability to take up riboflavin or its macromolecular conjugates, which is indicative of their expression of RFRs [20, 21, 26, 32, 42]. These cells include KB carcinoma [21, 26, 42], LnCap (prostate cancer) [20, 32], SK-LU-1 and A549 (lung cancer) [21], and SK-OV (ovarian cancer) [21]. In addition, a class of ATP-dependent RF transporters is involved in the subcellular accumulation of RF in certain cancer stem cells which are resistant to anticancer chemotherapeutic agents, suggesting their potential as a biomarker for these cells [43].

RFRs share several structural and functional similarities with FARs. Both RFRs and FARs belong to the family of folate binding proteins which are glycosylphosphatidylinositol-anchored surface receptors [38]. The receptors exhibit a high degree of homology in their amino acid sequences [44] and have similar secondary structure [45] in their ligand binding domains. RFRs, like FARs are taken up along with their bound ligand by the cell through endocytosis [21, 23, 46], the mechanism responsible for the uptake of NPs following their cell surface binding to the receptor.

Despite such similarities between these two important vitamin uptake receptors, RFRs play a distinct role in RF transport and cellular uptake and exist as more diverse forms such as soluble carriers, transporters, and membrane-bound proteins [23, 39, 40, 45]. As summarized in Table 7.1, RFRs also show clear differences in their tissue distribution and the types of malignant cells they are associated with including cancer stem cells [43]. Such distinct features of RFRs suggest an important opportunity for targeting specific malignant cells which are otherwise not addressable by use of other tumor biomarkers. In addition to their ligand role,

certain types of RF analogs display potent cytotoxic activity due to their ability to competitively interfere with the cellular functions of flavin cofactors [48], and offer additional benefits in the therapeutic applications of RF ligand-conjugated nanoplatforms [25].

7.2.2 *Riboflavin Ligands*

The primary targeting ligand for RFR-targeted platform design is RF which is the endogenous ligand for these receptors. It is made up of two structural units—an isoalloxazine and a (D)-ribose, each modifiable for ligand conjugation (Fig. 7.1). In addition, there are a number of structural homologues to RF which are referred to as RF antagonists or antimetabolites. These include roseoflavin, cofactor F_{420} [47], and 2(4)-imino-4(2)-amino-2,4-dideoxyriboflavin [25, 47–49]. Each of these retains the ability to bind RFRs, but lacks the requisite functional activity required for the biosynthesis of RF-associated cofactors.

To be considered ideal for the design of RFR-targeted platforms, the ligand should provide certain sites amenable for linker installation, allow easy synthetic modification, and lack any functional activity for stimulating cell growth. In an effort to identify such ligands, we searched RF-mimicking small molecules in the SciFinder® database, and identified a set of candidate molecules that include

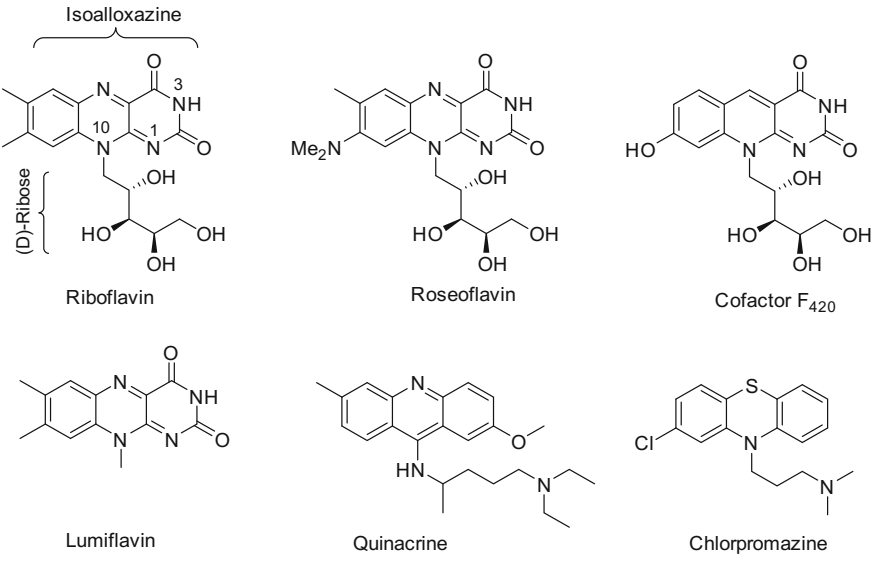

Fig. 7.1 Riboflavin and selected riboflavin antagonists which are either naturally occurring (roseoflavin, cofactor F_{420}, lumiflavin) or synthetic (quinacrine, chlorpromazine)

Table 7.2 Binding affinity and thermodynamic parameters of RF antagonists to riboflavin binding protein (RFBP) in PBS buffer, pH 7.4

RF antagonists	n^a	K_D (nM)	ΔH^a (kJ mol^{-1})	ΔG (kJ mol^{-1})	ΔS (kJ mol^{-1} K^{-1})
Riboflavin	0.78 ± 0.02	5.0	−91.2 ± 5.7	−47.5	−0.15
Lumiflavin	1.08 ± 0.07	61	−48.2 ± 7.2	−41.2	−0.02
Quinacrine	0.90 ± 0.04	264	−51.6 ± 3.9	−37.5	−0.05
Chloroquine	1.06 ± 0.04	2100	−40.4 ± 2.9	−32.4	−0.03
Perphenazine	No binding observed				
Chlorpromazine	No binding observed				

Adapted with permission from [25]. Copyright © 2011, American Chemical Society
[a]n = binding stoichiometry of ligand to receptor. Reported errors (SD) are from fitting data

perphenazine, chlorpromazine, quinacrine, and chloroquine (Fig. 7.1) [25]. Each of these is structurally less complex than RF but contains a flat tricyclic heterocycle that mimics the isoalloxazine head of RF.

We investigated the binding interaction of these small molecules with chicken RFBP using isothermal titration calorimetry (ITC), and determined their dissociation constants (K_D) as summarized in Table 7.2. In general, these molecules bound with lower affinity than RF in the order of RF (5.0 nM) > lumiflavin (61 nM) > quinacrine (264 nM) > chloroquine (2100 nM). Two other tested compounds, perphenazine and chlorpromazine, lacked detectable binding affinity despite their structural similarities based on the tricyclic heterocycle. Both lumiflavin and quinacrine do not cause undesired positive trophic effects as those associated with the function of RF which has been shown to stimulate tumor cell growth. Despite their lower affinity, it is anticipated that NPs conjugated with this lower affinity ligand will still have the ability to bind RFRs on the cell surface with high avidity constants via multivalent binding interactions [50–52]. Use of these RF-mimicking molecules in the design of RFR-targeted platforms constitutes a subject of follow-up studies.

7.3 Application of RF-Conjugated Dendrimers

7.3.1 Linker Design

An X-ray crystal structure was determined for RF in complex with chicken RFBP at a resolution of 2.5 Å [45]. This serves as the basis for rational linker design by providing several insights on the position and orientation of the linker needed in the design of a RF-linker construct. First, the xylene domain of its isoalloxazine unit is stacked between aromatic planes in the ligand binding cleft and is not ideal for linker attachment. However, the opposite face (*N*-3 position) of the same isoalloxazine head is relatively open for linker modifications. This is illustrated by an earlier study, in which 3-carboxymethylriboflavin (**1**, Fig. 7.2) [25, 53, 54], a RF derivative with a carboxylic acid extended out from the *N*-3 position, retained its

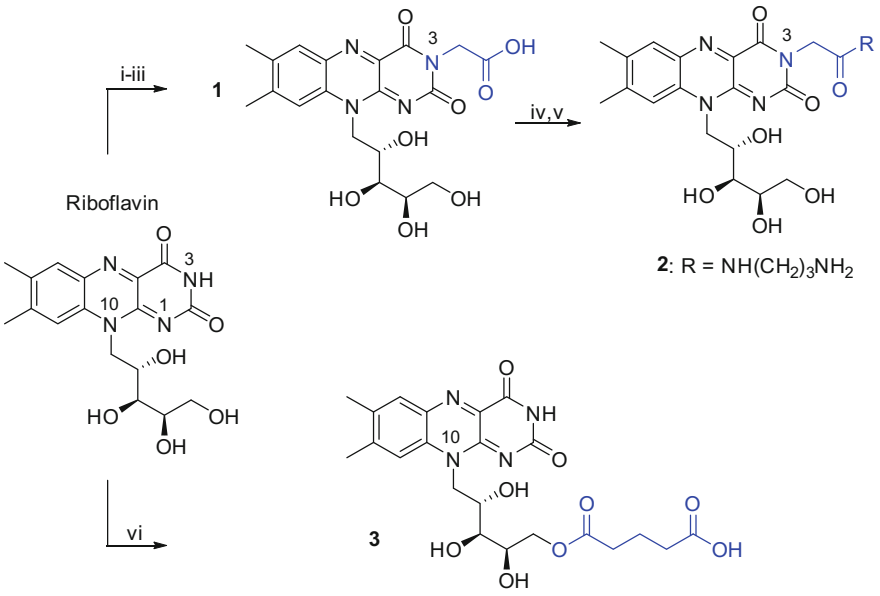

reagents and conditions: i) Ac_2O, AcOH,65°C, 6 h; ii) Ethyl bromoacetate (3 eq), K_2CO_3 (3 eq), DMF, 85°C; iii) 6 M HCl, 90°C, 6 h; iv) EDC, NHS, DMAP, DMF, rt; then N-Boc 1,3-diaminopropane; v) TFA, CH_2Cl_2, rt; vi) glutaric anhydride (2 eq), pyridine, DMSO.85°C, 12 h. rt = room temperature

Fig. 7.2 Synthesis of riboflavin linker constructs. Each linker (in *blue*) is installed at the *N*-3 (**1**, **2**) or *N*-10 position through the terminal hydroxyl group of (D)-ribose (**3**)

affinity for RFBP which allowed its use in the detection of RFBP in milk products [53, 54]. Synthesis of this riboflavin linker construct at the *N*-3 position (**1**) as described in literature [25, 53, 54] is conveniently achieved in three consecutive steps that comprise of the exhaustive acetylation of (−)-riboflavin, the *N*-alkylation of 2′,3′,4′,5′- tetra-*O*-acetylriboflavin to the ethoxycarbonyl methyl derivative, and complete removal of ester protecting groups by acidic hydrolysis (Fig. 7.2).

In order to further validate 3-carboxymethylriboflavin as the linker construct in RFR-targeted delivery platforms, we investigated its binding affinity to RFBP by surface plasmon resonance (SPR) spectroscopy using a biosensor chip prepared by immobilization with **2** which contains a spacer (3-aminopropyl) at the carboxylic acid terminus of 3-carboxymethylriboflavin. This amine-terminated riboflavin derivative **2** was prepared by the EDC-mediated amide conjugation of 3-carboxymethylriboflavin **1** with a mono *N*-Boc protected propanediamine (Fig. 7.2). RFBP bound to the surface in a dose-dependent manner (Fig. 7.3). Its binding was also ligand-specific, as the RFBP adsorption was competitively blocked by co-injecting RF, quinacrine and **2**. This SPR study validated the compatibility of the linker installation made at the *N*-3 position of RF.

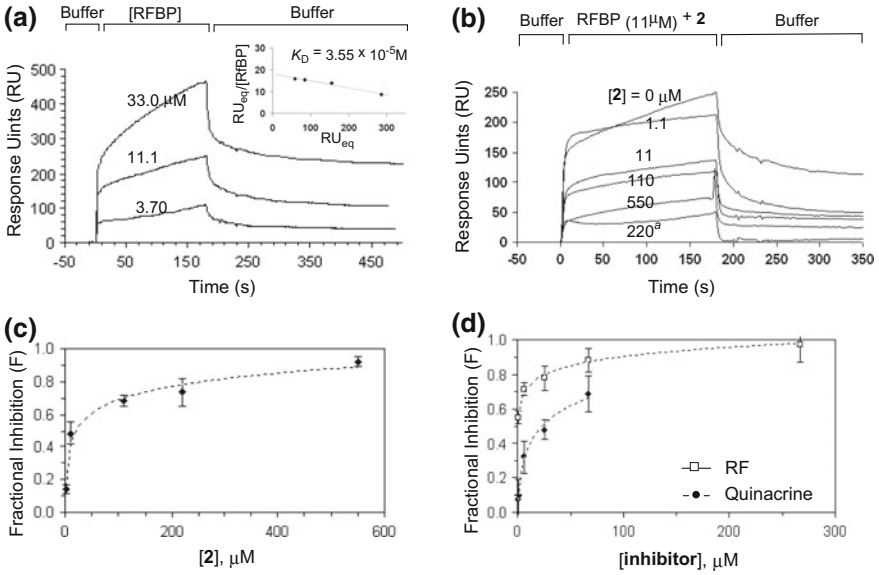

Fig. 7.3 Surface plasmon resonance (SPR) spectroscopy using a riboflavin (**2**)-immobilized CM5 sensor chip. **a** Binding of RFBP in PBS (pH 7.4). *Inset* a Scatchard plot; **b** Competitive binding experiments of riboflavin binding protein (RFBP) with **2**. [a]Injection of **2** alone (220 μM) without RFBP; **c**, **d** Plot of fractional inhibition ($F = 1 - (RU_{[I]}/RU_{[I]=0})$) as a function of the ligand (RF, **2**) or competitive inhibitor (quinacrine). Adapted with permission from [25]. Copyright © 2011, American Chemical Society

Second, the (D)-ribose unit is largely exposed to the aqueous medium and makes a minimal contribution to receptor binding. Thus, its external accessibility in combination with its flexible configuration makes the sugar unit suitable for linker installation as illustrated by a glutarate linker attached at the terminus of the (D)-ribose through an ester linkage (**3**, Fig. 7.2). This riboflavin derivative **3** contains a glutarate moiety attached through an ester linkage at its hydroxyl group of the (D)-ribose unit. It was prepared by heating a mixture of riboflavin and glutaric anhydride in a mixture of pyridine and DMSO. This coupling reaction might occur regioselectively at the primary hydroxyl group as suggested by other similar conjugation reactions of riboflavin reported elsewhere [21, 46], possibly because the primary terminal position is sterically less hindered than those secondary alcohols located adjacent to the bulky isoalloxazine head.

7.3.2 *Dendrimer Conjugates Designed for RFR-Targeted Drug Delivery*

We developed RF-targeted delivery platforms with a generation 5 (G5) poly(amidoamine) (PAMAM) dendrimer (diameter 5.4 nm) [55]. This PAMAM dendrimer

has a globular shape with a large number of dendritic branches (theoretically 128 for G5), each terminated with a primary amine which is amenable to conjugation with a targeting ligand or a drug molecule. The use of this G5 dendritic polymer provides several key benefits for biomedical applications [56, 57] as it displays biocompatibility, is characterized by favorable pharmacokinetic properties such as extended duration of circulation, and lacks immunogenicity [58–61].

Two types of conjugates were designed that include $G5(RF)_{6.3}(FITC)_{1.3}$ **5** and $G5(RF)_{2.5}(MTX)_{3.9}$ **6** (Fig. 7.4). First, $G5(RF)_{6.3}(FITC)_{1.3}$ is a fluorescently labeled conjugate that has a mean of 6.3 RF molecules and 1.3 fluorescein isothiocyanate (FITC) molecules attached on the dendrimer surface prepared for confocal microscopic imaging of its cellular uptake. Here, the ligand attachment was made conveniently through an ester bond formed between a primary hydroxyl group on the (D)-ribose unit of RF and a glutaric acid spacer presented on the dendrimer surface. Second, $G5(RF)_{2.5}(MTX)_{3.9}$ **6** is a drug conjugate that carries covalently attached

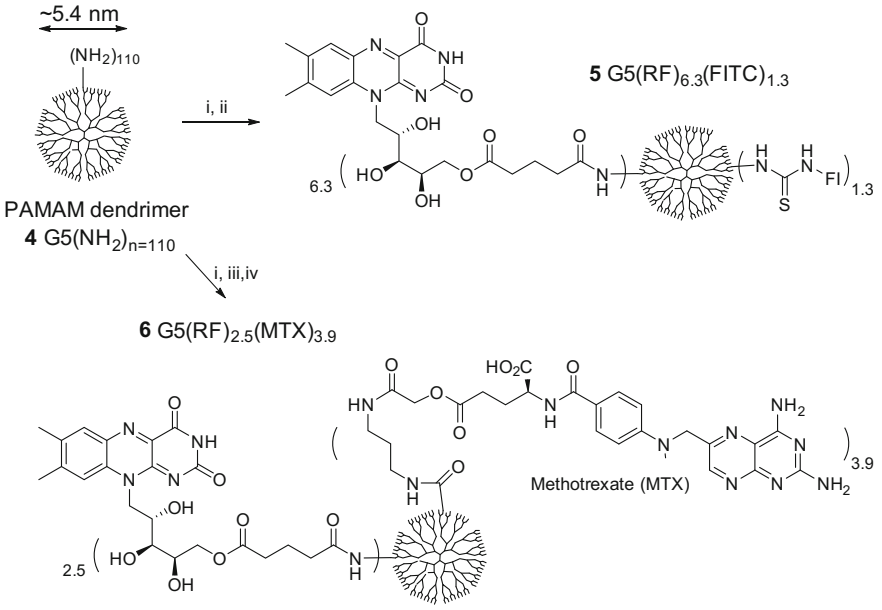

Reagents and conditions: (i) glutaric anhydride, Et_3N, MeOH, rt, 3 days; (ii) riboflavin, FITC-$NH(CH_2)_4NH_2$, EDC, DMAP, DMF, rt; (iii) EDC, 4-dimethylaminopyridine (DMAP), riboflavin, DMF, rt, 24 h; (iv) MTX-$C(=O)O(CH_2)_3NH_2$, EDC, DMAP, DMF, rt, 24 h

Fig. 7.4 Structure of a fifth generation (G5) poly(amidoamine) dendrimer $G5(NH_2)$ (**4**), and synthesis of two representative riboflavin (RF)-conjugated dendrimers, $G5(RF)_{n=6.3}(FITC)_{p=1.3}$ (**5**) and $G5(RF)_{n=2.5}(MTX)_{m=3.9}$ (**6**). *n*, *m* and *p*: each refers to a mean number of RF, methotrexate (MTX) or fluorescein isocyanate (FITC) covalently attached to the dendrimer polymer, respectively

methotrexate (MTX) as the payload. MTX potently inhibits dihydrofolate reductase in the cytoplasm with a K_i value of 4.8 pM [62], leading to strong inhibition of cell growth.

Assessment of the cellular binding and uptake of conjugate **5** was performed in RFR(+) KB cells. These cells belong to a subline of cervical tumor cells that showed receptor-mediated uptake of RF and RF-dye conjugates [21, 46]. Our flow cytometry analysis showed dose- and incubation time-dependent binding of the conjugate (Fig. 7.5) [26]. When incubated with other human cancer cell lines, this RF conjugate also showed significant fluorescence intensity in these cell lines including IGROV-1 (ovarian) and SCC15 (head and neck) like in KB cells. This is supportive of conjugate binding and uptake by these tumor cells, some of which have been validated earlier for their overexpression of RFR on the cell surface [21].

In a subsequent study, we investigated the effectiveness of this RFR-targeted conjugate for drug delivery using $G5(RF)_{2.5}(MTX)_{3.9}$ **6**. The cytotoxic effect of **6** was determined in KB cells in vitro using an XTT assay (Fig. 7.5b). This conjugate showed potent inhibition of tumor cell growth at low nM doses, and its inhibition activity was incubation time- and dose-dependent. The IC_{50} value estimated from

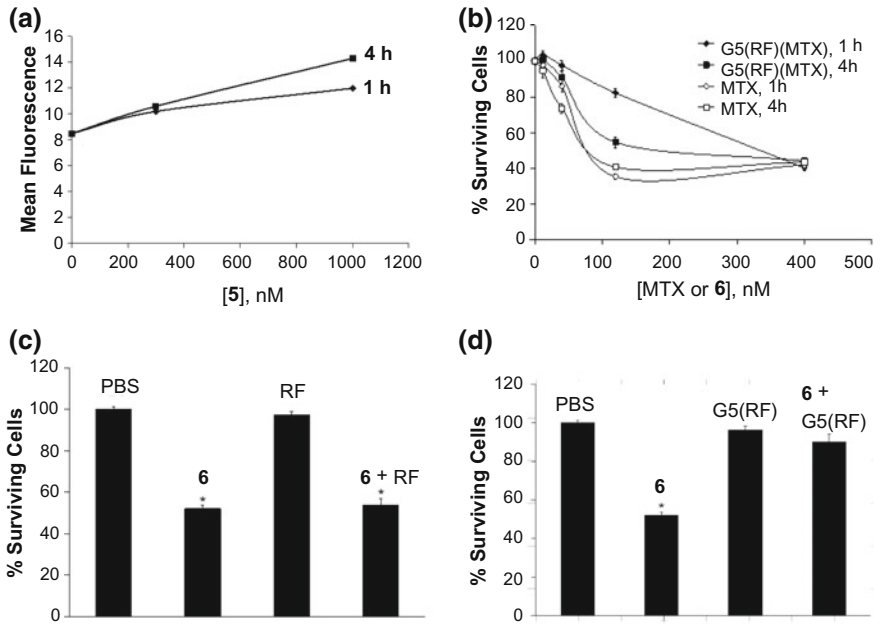

Fig. 7.5 **a** Dose-dependent binding and uptake of **5** $G5(RF)_{6.3}(FI)_{1.3}$ in KB cells (incubation time = 1, 4 h); **b** Dose-dependent cytotoxicity of **6** $G5(RF)_{2.5}(MTX)_{3.9}$ and free MTX in KB cells; **c** Effect of a competitive ligand (RF) on cell growth. PBS (control), **6** (30 nM), RF (30 μM), and **6** (30 nM) + RF (30 μM); **d** Effect of a RF-conjugated dendrimer on cell growth. PBS, **6** (30 nM), $G5(RF)_{2.5}$ (30 μM), and $G5(RF)_{2.5}$ (30 μM) + **6** (30 nM). *Asterisk* the *p* value for each of the data set is <0.005 compared to PBS. Reprinted with permission from [26]. Copyright © 2010, Elsevier

the dose response curve (at 4 h incubation) for the conjugate was 72 nM, which indicates slightly lower activity than that of free MTX of 48 nM.

In order to verify the mechanism of RF-mediated delivery by **6**, we performed a series of ligand competition experiments in RFR(+) KB cells with RF (30 μM, Fig. 7.5c) or $G5(RF)_{2.5}$ (30 μM, Fig. 7.5d). Here, the addition of RF or its dendrimer conjugate $G5(RF)_{2.5}$ (which has no MTX attached) alone showed no effect on cell growth. When $G5(RF)_{2.5}(MTX)_{3.9}$ **6** (30 nM) was co-incubated with an excess amount (30 μM) of $G5(RF)_{2.5}$ (a multivalent ligand competing for RFR), the cytotoxicity of **6** could be effectively blocked due to perhaps competitive occupation of RFRs by the added $G5(RF)_{2.5}$ which would contribute to the decrease of its intracellular uptake. As a result, the cell growth was restored to 90% from ~50% observed in the absence of $G5(RF)_{2.5}$.

Co-incubation with free RF failed to show such restoring effects on cell growth. This distinct difference between RF and $G5(RF)_{2.5}$ is attributable to the high avidity binding of the multivalent conjugate compared to the monovalent RF ligand [51, 52, 63]. Our results of ligand competition experiments are in agreement with a previous uptake study performed with ^{125}I-labeled, multivalent RF-conjugated bovine serum albumin (shortly, ^{125}I-$BSA(RF)_5$) in RFR(+) KB cells reported by Low et al. [21]. Thus, co-incubation of ^{125}I-$BSA(RF)_5$ with free RF (at 10–40 mol excess) resulted in almost no change in its cellular uptake relative to no RF addition, while co-incubation with an unlabeled $BSA(RF)_5$ (at 10 mol excess) led to significant blocking (~70%) of its uptake, evidence supportive of its multivalent tighter binding than monovalent RF.

All of these studies are supportive of the cellular uptake of **6** through a RFR-mediated mechanism and verify the activity of delivered MTX in the cytoplasm in inducing potent cytotoxicity. These studies also point to the potential application of RF-conjugated dendrimers in targeted delivery of a fluorescent imaging molecule and an anticancer therapeutic agent to malignant tumor cells overexpressing the RF receptor.

7.3.3 *Dendrimer Conjugates Designed for RFR-Targeted Gene Delivery*

We investigated the potential of applying RF-conjugated dendrimers as a new class of nonviral vectors for RFR-targeted gene delivery in tumor cells (Fig. 7.6) [42]. For this approach, we modified the conjugate $G5(RF)_{4.9}$ by co-attachment of multiple molecules of 3,8-diamino-6-phenylphenanthridinium (DAPP) which has the ability to intercalate into DNA, thus forming polyplexes with dsDNA. The resulting dendrimer $G5(RF)_{4.9}(DAPP)_{6.9}$ has dual functional motifs, one for targeting RFRs on the cell surface and the other for anchoring a DNA payload.

We selected a series of RF-conjugated dendrimers along with other targeted dendrimers that include **7** $G5(FA)_{8.6}$, **8** $G5(DAPP)_{5.4}$, **9** $G5(FA)_{8.6}(DAPP)_{5.4}$, **10** $G5(RF)_{4.9}$, and **11** $G5(RF)_{4.9}(DAPP)_{6.9}$. Each was used for preparing a series of

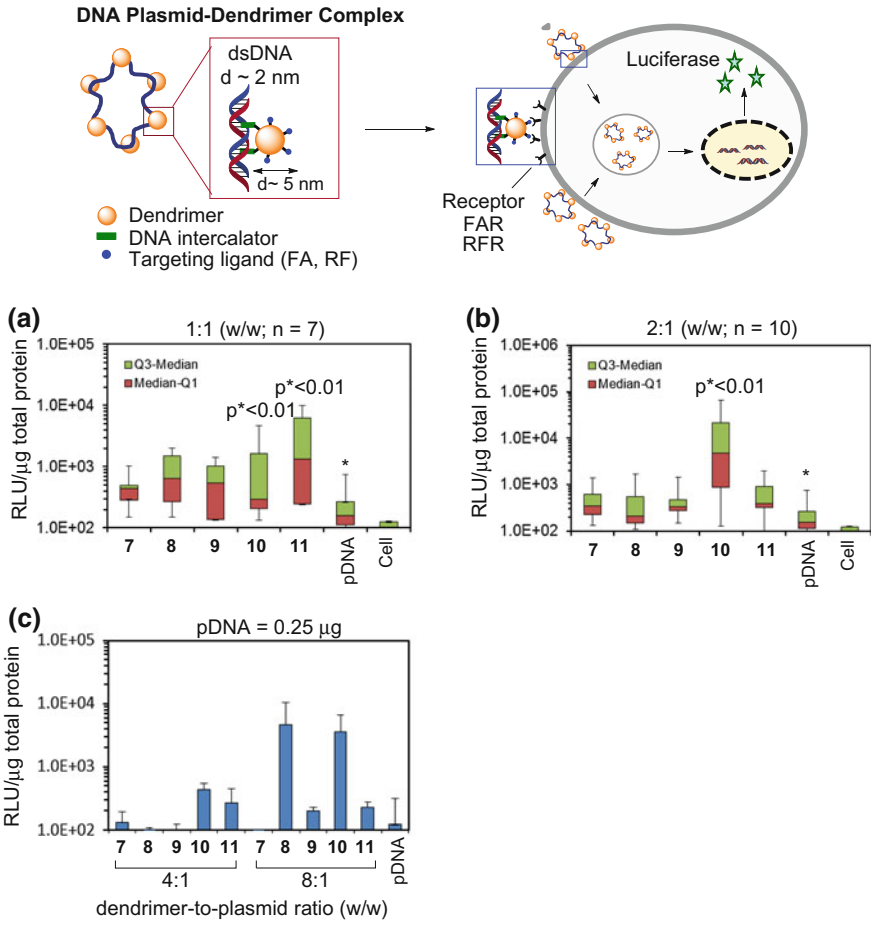

Fig. 7.6 A schematic illustrating the concept for dendrimer vectors with DNA intercalation motifs for RFR-targeted gene delivery. **a–c** Transfection of luciferase plasmid DNA (pLuc) in FAR(+) and RFR(+) KB cancer cells via dendrimer polyplexes, each made with **7** G5$(FA)_{8.6}$, **8** G5$(DAPP)_{5.4}$, **9** G5$(FA)_{8.6}(DAPP)_{5.4}$, **10** G5$(RF)_{4.9}$, and **11** G5$(RF)_{4.9}(DAPP)_{6.9}$. **a**, **b** *Box* and *whisker* plots showing the distribution of luminescence at dendrimer-to-plasmid (D/P) ratios of 1:1 (**a**) and 2:1 (**b**) at 1 µg of pLuc. Each *p* value was calculated against plasmid DNA alone (*Asterisk*). **c** Luciferase transfection at higher D/P ratio of 4:1 or 8:1. DAPP = 3,8-di-amino-6-phenylphenanthridine. *RLU* relative light unit. *Error bars* standard deviation (±SD). Adapted with permission from [42]. Copyright © 2011, American Chemical Society

polyplexes by complexation with plasmid DNA (pDNA) encoding a luciferase (pLuc) as a reporter gene. Several polyplexes containing DNA at various dendrimer-to-pDNA ratios (D/P) were made, and it was investigated whether such dendrimer polyplexes are effective for gene transfection by performing transfection experiments in FAR(+) and RFR(+) KB carcinoma cells in vitro.

As presented in Fig. 7.6a, b, each of the polyplexes prepared at the D/P ratios of 1:1 or 2:1 showed transfection activities greater than the pristine plasmid used as control. The transfection efficiency varied with dendrimer type such that polyplexes prepared with **10** G5$(RF)_{4.9}$ or **11** G5$(RF)_{4.9}(DAPP)_6$ gave the highest transfection efficiency at each ratio with statistical significance of $p < 0.01$ (F test). These were more effective than those polyplexes prepared with FA-conjugated dendrimers. It is notable that **10** G5$(RF)_{4.9}$ showed such high efficiency despite its lack of DAPP which was presumably needed for DNA anchoring. We postulate that RF alone attached to the dendrimer could play a dual functional role as both a targeting ligand and DNA anchor due to its previously demonstrated ability to intercalate its flat isoalloxazine head between two adjacent DNA base pairs in dsDNA [64, 65]. The efficiency of gene transfection also varied with the D/P ratios while a single best ratio applicable for all polyplexes was not observed. This variation is attributable to the mechanism of nonviral gene delivery [66] in which the ratio as well as nanoparticle type determine the shapes and charge properties of the polyplexes, each playing a critical role in the course of intracellular uptake, DNA release, and nuclear transport. This observation is indicative of the challenges in predicting the optimal structure and function of the polyplex which requires further studies in the future.

The cellular uptake of these polyplexes can occur through either FAR or RFR-mediated mechanism. By confocal microscopy, we imaged KB cells treated under the same conditions as in the transfection experiment. As shown in Fig. 7.7, cells treated with each polyplex showed significant fluorescence which is indicative of their cellular uptake. Most of the fluorescence intensity was predominantly localized in the cytoplasmic area rather than on the cell surface and with only minor fluorescence observed in the nuclei. This is supportive of their intracellular uptake possibly via a receptor-mediated mechanism, as well as the release of pDNA in the cytoplasm rather than nuclear uptake of the polyplex complex. As a comparison, **8** G5(DAPP) which lacks RF was taken up, but less effectively than **11** G5(RF)(DAPP), suggesting the possibility of other mechanisms of uptake such as macropinocytosis and phagocytosis which is dependent on nanoparticle shapes [67].

In summary, we investigated a new concept for targeted gene delivery using RF-conjugated multifunctional dendrimers. This novel platform was highly effective for facilitating gene transfection in specific for RFR(+) mammalian cells.

7.3.4 RFR-Targeted Imaging Methods

As shown above, imaging of RF-conjugated dendrimers in the cell can be performed by confocal microscopy by focusing on fluorescent dye molecules associated with the NP. However, these dye molecules are photounstable and rapidly bleach, leading to reduced resolution and detection capabilities. We developed another imaging modality for investigating the cellular association of RF-conjugated dendrimers [27]. It is based on a gold nanoparticle (AuNP) system

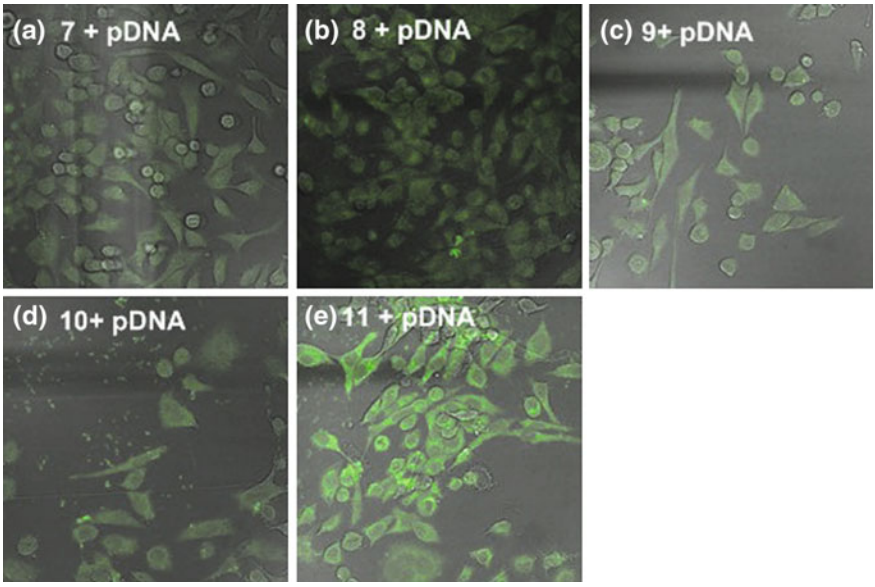

Fig. 7.7 **a**–**e** Fluorescence confocal microscopy of various polyplexes taken up by KB cells in vitro. Each sample was prepared using polyplexes made of luciferase plasmid (1 μg/mL) in complex with each of dendrimer conjugates **7** $G5(FA)_{8.6}$, **8** $G5(DAPP)_{5.4}$, **9** $G5(FA)_{8.6}(DAPP)_{5.4}$, **10** $G5(RF)_{4.9}$, or **11** $G5(RF)_{4.9}(DAPP)_{6.9}$ at a 2:1 ratio (w/w). In this imaging study, the localization of the dendrimer polyplex was detected by fluorescent emission that is attributed to excitation of dendrimer-attached ligands including folate (**a**), riboflavin (**d**), and/or DAPP (3,8-di-amino-6-phenylphenanthridine; **b**, **c**, **e**). Reprinted with permission from [42]. Copyright © 2011, American Chemical Society

which displays unique optophysical properties such as surface plasmon resonance (SPR) absorption, visible luminescence, and SPR scattering effects [68, 69]. With these modalities, the detection of AuNP does not require conjugation with any additional fluorescent labels, and it is conveniently performed under dark field light [70–72] and confocal microscopy [73].

The AuNPs used in this study [27] were spherical in shape and displayed a maximal absorption (λ_{max}) band at 520 nm. The size distribution of AuNPs was measured by atomic force microscopy (AFM), indicating a mean diameter of 13.5 ± 2.2 nm. Their hydrodynamic diameter as determined by dynamic light scattering (DLS) was as large as ~ 30 nm (Z_{ave}) which points to the contribution of the hydrated diffusion layer surrounding the AuNP core to the measured size. The AuNP was modified to form the core–shell nanocomposite AuNP@dendrimer by its surface modification with dendrimer conjugates **12**, **13** $G5(RF)_n$ ($n = 0, 4$) (Fig. 7.8). The surface modification was achieved through Au–S chemisorption between the surface Au and the cyclic disulfide moiety at the terminus of a lipoic amide branch of the dendrimer.

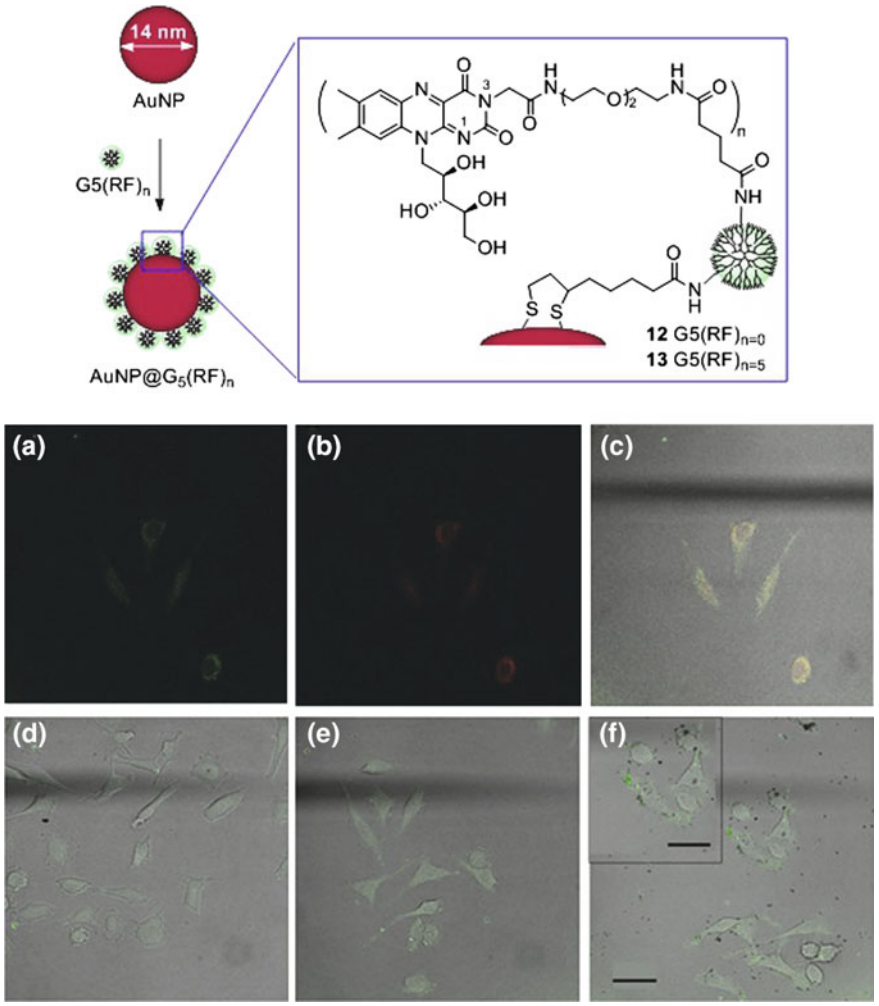

Fig. 7.8 SPR scattering imaging for the cellular uptake of dendrimer-coated gold nanoparticles AuNP@G5(RF)$_n$ in KB cells. **a–c** KB cells treated with 50 nM of unmodified AuNP for 2 h were imaged by **a** SPR scattering or **b** luminescence. **c** Co-localization of the signals was confirmed by the overlay. SPR scattering imaging was taken for KB cells treated for 4 h with 80 nM of **d** AuNP, **e** AuNP@G5(RF)$_{n=0}$ or **f** AuNP@G5(RF)$_{n=5}$, (*inset* is a magnified view of the adjacent cells). *Scale bar* 30.3 μm (*inset*, 28.8 μm). Signal from the SPR scattering was overlaid with differential interference contrast (DIC) images. Reprinted with permission from [27]. Copyright © 2014, American Chemical Society

We first validated two methods for detecting AuNPs which did not contain any fluorescent dyes or chemisorbed dendrimer. As shown in Fig. 7.8a–c, RFR(+) KB cells were incubated with citrate-stabilized AuNPs (50 nM) for 2 h, and were imaged by confocal microscopy via two detection modes including SPR scattering

(λ_{ex} 514 nm; λ_{em} 474–506 and 522–570 nm) and luminescence (λ_{ex} at 514 nm; λ_{em} at 550–650 nm). AuNPs associated with the cells were clearly detectable under both detection modes, SPR (Fig. 7.8a) and luminescence (Fig. 7.8b); however, their detection intensities were rather weak due to their low level of cellular uptake.

For enhanced uptake, KB cells were treated at a slightly higher concentration (80 nM) and incubated for a longer period (4 h) with AuNP and AuNP@G5(RF)$_n$ (n = 0, 5). Images of the treated cells were acquired in the SPR scattering mode, showing qualitatively clear differences between untargeted NPs (AuNP, AuNP@G5(RF)$_0$) and targeted AuNP@G5(RF)$_5$. The targeted AuNP@G5(RF)$_5$ showed more punctate and localized areas of signal, and their intensity was distinctly greater than those observed otherwise with the bare unmodified AuNP as well as with the AuNP@G5(RF)$_0$) treated cells (Fig. 7.8d–f). We attribute this scattering detection to large aggregates of AuNPs rather than individual AuNPs either bound on the cell surface or internalized.

In summary, our confocal microscopy studies demonstrated the utility of the dual detection modes of SPR scattering and luminescence for the determination of the cellular localization of dendrimer-chemisorbed AuNPs in tumor cells. As covalent modification with fluorophores for detection is sometimes not desirable due to the possible alteration of native activity, these nonfluorescent-based methods of detection may offer a better alternative for imaging applications.

7.4 Biophysical Basis of Multivalent High Avidity

The design principle of targeted NPs involves a multivalent ligand system in which each NP is conjugated with multiple targeting ligands. Thus, the multivalent NP recognizes and binds to a target cell with high specificity and strong binding affinity, which together are referred to as avidity [51, 52, 63, 74]. Unlike affinity which often refers to the strength of monovalent interaction between a single receptor and ligand pair, avidity is a collective property that measures the strength of simultaneous interactions between multiple receptor–ligand pairs [51, 56, 57] (Fig. 7.9).

Multivalent design factors have been extensively investigated by many laboratories including ours by conjugation of small molecule ligands such as carbohydrates [51, 63, 75, 76], folate [77, 78], methotrexate [79–83], vancomycin [84–87], and oligonucleotide [88] to NP scaffolds based on polymers [75, 89, 90], dendrimers [77, 79, 84, 88], and inorganic nanomaterials [78, 86, 87, 91]. These studies suggest that several factors play a significant role in conferring high avidity and selectivity. These include: (1) use of threshold ligand valence [77, 84, 88]; (2) presentation of two different ligands for co-targeting two distinct receptors on the same cell surface [78, 91]; (3) evaluation of NP sizes and shapes [92] for optimized conformal interactions [75, 93, 94]. It is also notable that an overcrowding or steric effect can occur [89, 95] when too many or bulky ligands are presented on the same surface of a NP which thus can interfere with high avidity

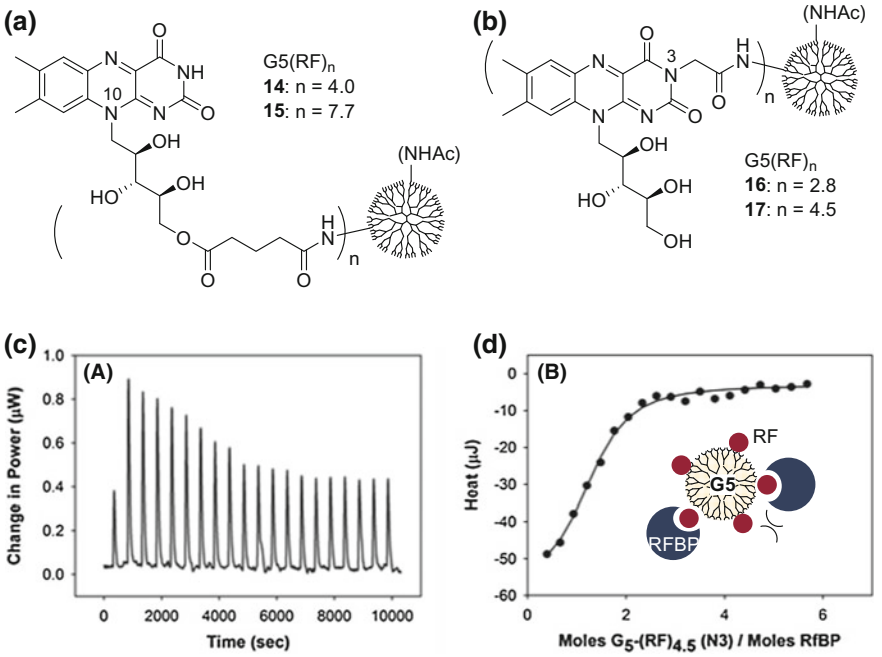

Fig. 7.9 **a**, **b** Structures of two RF-conjugated dendrimer series G5(RF)$_n$. In each, the RF ligand is tethered to the G5 PAMAM dendrimer through a linker located at either its *N*-10 or *N*-3 position with variable valency (*n*). **c** Representative raw ITC data for the interaction between **17** G5(RF)$_{4.5}$ with chicken RFBP (4 μM) at 25 °C in PBS buffer. **d** Plot of integrated area under each injection peak for **17**. The *solid line* is an independent model fit to data with parameters *n*, K_D, and ΔH. *Inset* a model for monovalent receptor–ligand association. Reprinted with permission from [28]. Copyright © 2012, American Chemical Society

binding. This steric interference is especially an issue with large molecule ligands such as antibodies [96]. Here, we investigated the biophysical basis for the specific and high avidity adsorption of RF-conjugated dendrimers to receptor expressing cell surfaces.

7.4.1 Ligand Affinity

We first investigated the thermodynamic basis of monovalent interactions between a receptor and a RF-conjugated dendrimer in solution [51]. One of the key design factors of this dendrimer conjugate is the RF valency which is known to play a significant role in controlling the avidity of the multivalent system. However, little is known about its role in monovalent affinity. Two series of RF-conjugated dendrimers G5(RF)$_n$ **14**–**19** were prepared by the covalent attachment of RF at either its *N*-10 or *N*-3 position to the dendrimer (Fig. 7.9). The linker used for RF attachment

in each series is composed of a three to five atom spacer. We chose this linker length as our previous cell binding [26] and SPR studies [25] suggested that it is long and flexible enough for the dendrimer-attached RF to be able to dock in the ligand site of RFBP. In each series, the average number (n = valency) of RF attached was varied in order to determine whether the ligand valency plays any role in the monovalent affinity (K_D) of the tethered RF ligand in solution.

Several binding parameters for the interaction between RF-conjugated dendrimers and soluble RFBP were determined by ITC in solution as summarized in Table 7.3 [28]. First, free RF binds to RFBP with a binding stoichiometry (n_b) of 1:1 (RFBP/ligand) [25]. Each of **14–16** G5(RF)$_n$ in the *N*-10 series showed an n_b of ~3–5:1 (RFBP/dendrimer), indicative of partial occupation of all the RF sites on the dendrimer by RFBP. This stoichiometry is in close agreement with the analysis based on a simple sphere model in which approximately six to seven RFBP (d = 4–5 nm) protein molecules can be theoretically accommodated around the surface of a G5 dendrimer nanoparticle (d = 5.4 nm) [55]. In contrast, **17–19** G5(RF)$_n$ in which each RF was tethered through a short spacer (3 atom) at its *N*-3 position showed only 1–2 RFBP occupation per dendrimer. These results suggest that ligand conjugation at the (D) ribose terminus via a longer glutarate linker provides more space and flexibility for more optimal protein accommodation.

Overall, this ITC analysis suggests a number of new insights in multivalent ligand design. First, we observed an upper limit in the maximal number of ligands that could engage in receptor binding. Control of this limit is dependent on design factors such as linkage position, spacer length, and ligand valency. However, it is notable that the RFBP used here is a monovalent system in solution, and thus different from RFRs presented on the cell surface. Accordingly, the remaining unoccupied ligands on the dendrimer are still available for making opportunistic receptor binding interactions to these RFRs, given their proximity [28].

Second, the dissociation constant (K_D) values determined for all dendrimer conjugates were greater by a factor of 93–1110 relative to the K_D value of RF (5 nM) [25]. This suggests that the mean affinity of each RF ligand to RFBP is significantly decreased once it is conjugated to the dendrimer surface. The K_D values determined for the *N*-3 linkage series also showed reduced affinity to RFBP, but overall higher affinity by a factor of ~5 than the *N*-10 series at a similar RF valency. These results clearly signify that contacts made in the binding pocket by the RF ligand with an unmodified (D) ribose moiety are important, and thus contribute to tighter binding in the binding pocket.

Third, the decrease in the affinity of the RF-dendrimer conjugates to RFBP is better understood by examination of thermodynamic parameters based on enthalpic (ΔH) and entropic ($-T\Delta S$) contributions. Enthalpically, the binding of the *N*-3 conjugates was much more favorable than the *N*-10 series. In contrast, the entropic penalty ($-T\Delta S$) was more severe for the *N*-3 conjugates. This implies that the binding of the *N*-3 conjugates is largely enthalpy driven, and the conjugation of more RF ligands per dendrimer likely results in the higher entropic penalty perhaps due to steric repulsion or congestion [97].

Table 7.3 Thermodynamic parameters for the monovalent binding of RF-conjugated dendrimers with RFBP in solution (phosphate buffered saline, pH 7.4) at 25 °C

System (versus RFBP)	Linkage position	n_b	K_D (nM)	ΔH^a (kJ mol^{-1})	ΔG (kJ mol^{-1})	$^{-}T\Delta S$ (kJ mol^{-1})
G5(RF)$_0$	–	NB	NB	NB	NB	NB
14 G5(RF)$_{4.0}$	*N*-10	2.88 ± 0.27	2671 ± 199	−15.7 ± 2.3	−31.9	−16.3
15 G5(RF)$_{7.7}$	*N*-10	5.16 ± 0.76	4049 ± 13	−9.0 ± 2.2	−30.8	−21.8
16 G5(RF)$_{2.8}$	*N*-3	1.76 ± 0.06	465 ± 12	−41.0 ± 2.7	−36.2	4.8
17 G5(RF)$_{4.5}$	*N*-3	1.24 ± 0.06	568 ± 95	−55.7 ± 3.8	−35.3	20.4

Reprinted with permission from [28]. Copyright © 2012, American Chemical Society

n_b = Binding stoichiometry (RFBP/dendrimer). NB = no binding. Errors are reported to two standard deviations (SD)

[a]Reported errors are from fitting data

7.4.2 *Multivalent Avidity*

Our thermodynamic studies above show that the monovalent interaction between the RF-dendrimer conjugate and the RFBP in solution is not enhanced, but is in fact weaker than that of free RF. We then investigated the avidity of the multivalent binding interactions between a RF-conjugated dendrimer and multiple RFBP molecules presented on a surface (a model system of the cell surface). We employed AFM because of its proven ability to quantify multivalent effects in biomolecules and synthetic model systems [98]. In particular, AFM-based dynamic force spectroscopy allows for the precise measurement of the physical forces involved in biomolecular interactions [98].

We hypothesized that the multivalent avidity, which results from multiple, cooperative interactions, should result in a force which is greater to break than the monovalent affinity [51, 52, 63, 99]. For this AFM study, a model system for the cell surface was generated by immobilization of RFBP onto a substrate (an ultra-flat gold surface) as illustrated in Fig. 7.10. Force experiments were performed through the contact approach of an AFM tip coated with $G5(RF)_n$ (n = 0, 3, 5) to the RFBP-immobilized substrate followed by retraction to measure the rupture force arising from the recognition interaction. Rupture events were observed over the course of the tip retraction, and the binding specificity was confirmed by addition of a competitive ligand (free RF) (not shown) which led to the block of the rupture events.

For data analysis, rupture forces were extracted by force–distance curves as illustrated for $G5(RF)_5$ in Fig. 7.10, and those forces measured for $G5(RF)_n$ were plotted as a function of loading rates as shown in Fig. 7.10D. $G5(RF)_0$ showed only nonspecific, weak interactions as most of its rupture events showed lack of loading rate dependency as typically expected for nonspecific events. However, some events showed a small loading rate dependency which is believed to arise from nonspecific global interactions such as electrostatic and/or van der Waals interactions between the dendritic residues and the RFBP protein. $G5(RF)_3$ showed a loading rate dependency that was markedly different from the nonspecific interactions observed in $G5(RF)_0$. Its rupture forces were in the range of 40–50 pN which may arise from a combination of mono, di- or trivalent interactions given its ligand distribution [100]. $G5(RF)_5$ also showed a loading rate dependency that was different from $G5(RF)_3$. The rupture forces observed from the $G5(RF)_5$-RFBP interactions are higher, and in the range of 70–110 pN, and the upper end of these forces are most likely arising from multivalent binding greater than those in $G5(RF)_3$. It is notable that the rupture forces measured in $G5(RF)_5$ are greater than those in $G5(RF)_3$, and even comparable to the force ($\sim$75 pN) reported for a biotin-avidin bond ($K_D \sim 10^{-15}$ M) [101] which constitutes one of the strongest non-covalent interactions.

In summary, this dynamic force spectroscopy study enabled us to quantitatively measure the physical forces involved in the adsorption of RF-conjugated dendrimers to the surface through multivalent receptor binding. RF valency is

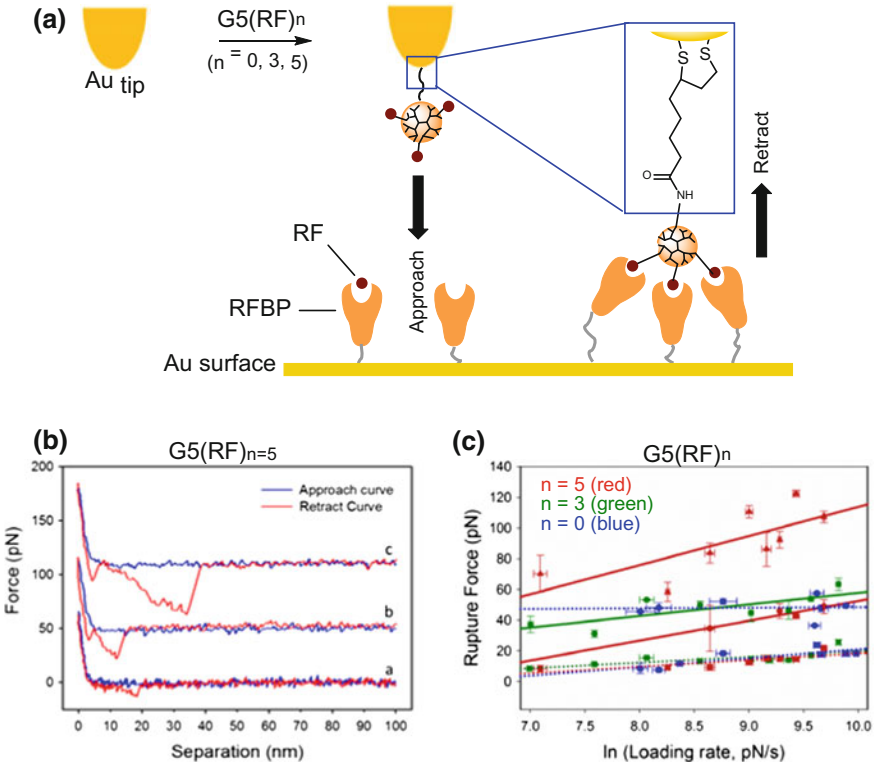

Fig. 7.10 **a** An AFM gold (Au) probe tip prepared by surface coating with G5(RF)$_n$ (n = 0, 3, 5; linkage at N-3 position), and schematic for dynamic force spectroscopy; **b** Representative force–distance curves between a G5(RF)$_5$ (**13**)-coated tip and RFBP covalently attached to an ultra-flat gold surface. Loading rate = 5.7 nN/s. Offset force curves depict rupture events in the **a** 10–20 pN, **b** 20–50 pN, and **c** 50–120 pN ranges; **c** Dynamic force spectra of G5(RF)$_n$ (n = 0, 3, 5) versus loading rate. *Square data* points represent rupture of unbinding event (**a**). *Circle* and *triangle* points represent unbinding events (**b**, **c**), respectively. Adapted with permission from [24]. Copyright © 2014, American Chemical Society

positively correlated with the magnitude of rupture force for dendrimer adhesion. These results were strongly supportive of its essential role in the design of RFR-targeted NPs.

7.5 Conclusion

RFR plays an essential role in cellular uptake of RF in normal physiology. Its overexpression is, however, observed in a number of cancer cell types and in cancer stem cells [19, 20, 43]. Here, we summarized the proof of concept studies reported

by our laboratories which demonstrated that RF or its homologous antagonists such as lumiflavin and quinacrine [25] have a strong potential to serve as ligands for selectively targeting RFRs, specific biomarkers in tumors and cancer stem cell biology. With a rational design approach based on an available RFBP crystal structure [45], we developed linker chemistry which enabled efficient conjugation of RF at its (D)-ribose unit and isoalloxazine head without loss of its binding activity [26, 28]. A series of multifunctional RF conjugates prepared with G5 PAMAM dendrimer were demonstrated as effective nanoplatforms for RFR-targeted delivery in RFR(+) KB cells in vitro using an anticancer therapeutic agent (MTX) and a reporter gene. Imaging methods based on AFM and confocal microscopy in combination with the SPR scattering modality of AuNPs conferred an ability to investigate the receptor-mediated uptake of RF-conjugated dendrimers by tumor cells [27, 42].

Development of nanotechnology for RFR-targeted applications has started only recently following early studies on receptor-mediated uptake of RF and its protein conjugates by tumor cells [21, 23]. Despite its early stage, a number of explorative studies which have been conducted in our laboratories [24–28] and others [29–31] are strongly supportive of multiple promising applications. These include delivery of antitumor agents (MTX [26], mitomycin C [31]) by RF-conjugated nanomaterials based on the PAMAM dendrimer [26, 28, 42], AuNP [27], *N*-(2-hydroxypropyl) methacrylamide (HPMA) copolymer [31], and human serum albumin [21]. In conclusion, we anticipate that RFR-targeted nanotechnology has a strong potential for playing a critical role in the development of new technology and effective nanodevices for tumor-specific delivery and imaging applications.

Acknowledgements The authors wish to acknowledge the support from the Michigan Nanotechnology Institute for Medicine and Biological Sciences, University of Michigan Medical School. SKC acknowledges partial support from the British Council and Department for Business Innovation and Skills through Global Innovation Initiative. KS acknowledges partial support from a Calvin College Research Fellowship.

References

1. Peer D, Karp JM, Hong S, Farokhzad OC, Margalit R, Langer R (2007) Nanocarriers as an emerging platform for cancer therapy. Nat Nanotechnol 2(12):751–760
2. Wong PT, Choi SK (2015) Mechanisms of drug release in nanotherapeutic delivery systems. Chem Rev (Washington, DC, US) 115(9):3388–3432
3. Kamaly N, Xiao Z, Valencia PM, Radovic-Moreno AF, Farokhzad OC (2012) Targeted polymeric therapeutic nanoparticles: design, development and clinical translation. Chem Soc Rev 41(7):2971–3010
4. Maeda H (2001) The enhanced permeability and retention (EPR) effect in tumor vasculature: the key role of tumor-selective macromolecular drug targeting. Adv Enzyme Regul 41(1):189–207
5. Zhu J, Shi X (2013) Dendrimer-based nanodevices for targeted drug delivery applications. J Mater Chem B 1(34):4199–4211

6. Esmaeili F, Ghahremani MH, Ostad SN, Atyabi F, Seyedabadi M, Malekshahi MR, Amini M, Dinarvand R (2008) Folate-receptor-targeted delivery of docetaxel nanoparticles prepared by PLGA–PEG–folate conjugate. J Drug Targ 16(5):415–423
7. Kelemen LE (2006) The role of folate receptor α in cancer development, progression and treatment: cause, consequence or innocent bystander? Int J Cancer 119(2):243–250
8. Yang W, Cheng Y, Xu T, Wang X, Wen L-P (2008) Targeting cancer cells with biotin-dendrimer conjugates. Eur J Med Chem 44:862–868
9. Yellepeddi VK, Kumar A, Palakurthi S (2009) Biotinylated poly(amido)amine (PAMAM) dendrimers as carriers for drug delivery to ovarian cancer cells in vitro. Anticancer Res 29 (8):2933–2943
10. Kok RJ, Schraa AJ, Bos EJ, Moorlag HE, Asgeirsdottir SA, Everts M, Meijer DKF, Molema G (2002) Preparation and functional evaluation of RGD-modified proteins as $\alpha_v\beta_3$ integrin directed therapeutics. Bioconj Chem 13(1):128–135
11. Pinto JT, Suffoletto BP, Berzin TM, Qiao CH, Lin S, Tong WP, May F, Mukherjee B, Heston WD (1996) Prostate-specific membrane antigen: a novel folate hydrolase in human prostatic carcinoma cells. Clin Cancer Res 2(9):1445–1451
12. Silver DA, Pellicer I, Fair WR, Heston WD, Cordon-Cardo C (1997) Prostate-specific membrane antigen expression in normal and malignant human tissues. Clin Cancer Res 3(1): 81–85
13. Ross JS, Fletcher JA (1998) The HER2/neu oncogene in breast cancer: prognostic factor, predictive factor, and target for therapy. Oncologist 3:237–252
14. Arteaga CL (2002) Epidermal growth factor receptor dependence in human tumors: more than just expression? Oncologist 7(suppl 4):31–39
15. Haugsten EM, Wiedlocha A, Olsnes S, Wesche J (2010) Roles of fibroblast growth factor receptors in carcinogenesis. Mol Cancer Res 8(11):1439–1452
16. Pollak M (2012) The insulin receptor/insulin-like growth factor receptor family as a therapeutic target in oncology. Clin Cancer Res 18(1):40–50
17. Herbison CE, Thorstensen K, Chua ACG, Graham RM, Leedman P, Olynyk JK, Trinder D (2009) The role of transferrin receptor 1 and 2 in transferrin-bound iron uptake in human hepatoma cells. Am J Physiol Cell Physiol 297(6):C1567–C1575
18. Bareford LM, Swaan PW (2007) Endocytic mechanisms for targeted drug delivery. Adv Drug Deliv Rev 59(8):748–758
19. Karande AA, Sridhar L, Gopinath KS, Adiga PR (2001) Riboflavin carrier protein: a serum and tissue marker for breast carcinoma. Int J Cancer 95:277–281
20. Johnson T, Ouhtit A, Gaur R, Fernando A, Schwarzenberger P, Su J, Ismail MF, El-Sayyad HI, Karande A, Elmageed ZA, Rao P, Raj M (2009) Biochemical characterization of riboflavin carrier protein (RCP) in prostate cancer. Front Biosci Landmark Ed 14:3634–3640
21. Holladay SR, Yang Z-F, Kennedy MD, Leamon CP, Lee RJ, Jayamani M, Mason T, Low PS (1999) Riboflavin-mediated delivery of a macromolecule into cultured human cells. Biochim Biophys Acta Gen Subj 1426(1):195–204
22. Phelps MA, Foraker AB, Gao W, Dalton JT, Swaan PW (2004) A novel rhodamine-riboflavin conjugate probe exhibits distinct fluorescence resonance energy transfer that enables riboflavin trafficking and subcellular localization studies. Mol Pharm 1(4):257–266
23. Huang S-N, Swaan PW (2000) Involvement of a receptor-mediated component in cellular translocation of riboflavin. J Pharmacol Exp Ther 294(1):117–125
24. Leistra AN, Han JH, Tang S, Orr BG, Banaszak Holl MM, Choi SK, Sinniah K (2015) Force spectroscopy of multivalent binding of riboflavin-conjugated dendrimers to riboflavin binding protein. J Phys Chem B 119(18):5785–5792
25. Plantinga A, Witte A, Li M-H, Harmon A, Choi SK, Banaszak Holl MM, Orr BG, Baker JR Jr, Sinniah K (2011) Bioanalytical screening of riboflavin antagonists for targeted drug delivery: a thermodynamic and kinetic study. ACS Med Chem Lett 2(5):363–367

26. Thomas TP, Choi SK, Li M-H, Kotlyar A, Baker JR Jr (2010) Design of riboflavin-presenting PAMAM dendrimers as a new nanoplatform for cancer-targeted delivery. Bioorg Med Chem Lett 20:5191–5194
27. Witte AB, Leistra AN, Wong PT, Bharathi S, Refior K, Smith P, Kaso O, Sinniah K, Choi SK (2014) Atomic force microscopy probing of receptor-nanoparticle interactions for riboflavin receptor targeted gold-dendrimer nanocomposites. J Phys Chem B 118(11): 2872–2882
28. Witte AB, Timmer CM, Gam JJ, Choi SK, Banaszak Holl MM, Orr BG, Baker JR, Sinniah K (2012) Biophysical characterization of a riboflavin-conjugated dendrimer platform for targeted drug delivery. Biomacromol 13:507–516
29. Beztsinna N, Solé M, Taib N, Bestel I (2016) Bioengineered riboflavin in nanotechnology. Biomaterials 80:121–133
30. Marlin F, Simon P, Bonneau S, Alberti P, Cordier C, Boix C, Perrouault L, Fossey A, Saison-Behmoaras T, Fontecave M, Giovannangeli C (2012) Flavin conjugates for delivery of peptide nucleic acids. ChemBioChem 13(17):2593–2598
31. Bareford LM, Avaritt BR, Ghandehari H, Nan A, Swaan PW (2013) Riboflavin-targeted polymer conjugates for breast tumor delivery. Pharm Res 30(7):1799–1812
32. Jayapaul J, Arns S, Bunker M, Weiler M, Rutherford S, Comba P, Kiessling F (2016) In vivo evaluation of riboflavin receptor targeted fluorescent USPIO in mice with prostate cancer xenografts. Nano Res 9(5):1319–1333
33. Lu Y, Low PS (2002) Folate-mediated delivery of macromolecular anticancer therapeutic agents. Adv Drug Deliv Rev 54(5):675–693
34. Low PS, Henne WA, Doorneweerd DD (2008) Discovery and development of folic-acid-based receptor targeting for imaging and therapy of cancer and inflammatory diseases. Acc Chem Res 41(1):120–129
35. Wang H-L, Wang S-S, Song W-H, Pan Y, Yu H-P, Si T-G, Liu Y, Cui X-N, Guo Z (2015) Expression of prostate-specific membrane antigen in lung cancer cells and tumor neovasculature endothelial cells and its clinical significance. PLoS ONE 10(5):e0125924
36. Shukla R, Thomas TP, Peters JL, Desai AM, Kukowska-Latallo J, Patri AK, Kotlyar A, Baker JR (2006) HER2 specific tumor targeting with dendrimer conjugated anti-HER2 mAb. Bioconj Chem 17(5):1109–1115
37. Mamot C, Drummond DC, Greiser U, Hong K, Kirpotin DB, Marks JD, Park JW (2003) Epidermal growth factor receptor (EGFR)-targeted immunoliposomes mediate specific and efficient drug delivery to EGFR- and EGFRvIII-overexpressing tumor cells. Cancer Res 63 (12):3154–3161
38. Foraker AB, Khantwal CM, Swaan PW (2003) Current perspectives on the cellular uptake and trafficking of riboflavin. Adv Drug Deliv Rev 55(11):1467–1483
39. Wu AML, Dedina L, Dalvi P, Yang M, Leon-Cheon J, Earl B, Harper PA, Ito S (2016) Riboflavin uptake transporter Slc52a2 (RFVT2) is upregulated in the mouse mammary gland during lactation. Am J Physiol Regul Integr Comp Physiol 310(7):R578–R585
40. Yonezawa A, Inui K-I (2013) Novel riboflavin transporter family RFVT/SLC52: identification, nomenclature, functional characterization and genetic diseases of RFVT/SLC52. Mol Aspects Med 34(2–3):693–701
41. White HB, Merrill AH (1988) Riboflavin-binding proteins. Annu Rev Nutr 8(1):279–299
42. Wong PT, Tang K, Coulter A, Tang S, Baker JR, Choi SK (2014) Multivalent dendrimer vectors with DNA intercalation motifs for gene delivery. Biomacromol 15(11):4134–4145
43. Miranda-Lorenzo I, Dorado J, Lonardo E, Alcala S, Serrano AG, Clausell-Tormos J, Cioffi M, Megias D, Zagorac S, Balic A, Hidalgo M, Erkan M, Kleeff J, Scarpa A, Sainz B Jr, Heeschen C (2014) Intracellular autofluorescence: a biomarker for epithelial cancer stem cells. Nat Methods 11(11):1161–1169
44. Zheng DB, Lim HM, Pène JJ, White HB (1988) Chicken riboflavin-binding protein. cDNA sequence and homology with milk folate-binding protein. J Biol Chem 263(23): 11126–11129

45. Monaco HL (1997) Crystal structure of chicken riboflavin-binding protein. EMBO J 16(7): 1475–1483
46. Huang S-N, Phelps MA, Swaan PW (2003) Involvement of endocytic organelles in the subcellular trafficking and localization of riboflavin. J Pharmacol Exp Ther 306(2):681–687
47. Mack M, Grill S (2006) Riboflavin analogs and inhibitors of riboflavin biosynthesis. Appl Microbiol Biotechnol 71(3):265–275
48. Chu CK, Bardos TJ (1977) Synthesis and inhibition analysis of 2(4)-imino-4(2)-amino-2,4-dideoxyriboflavin, a dual antagonist of riboflavin and folinic acid. J Med Chem 20(2):312–314
49. Musser EA, Heinle RW (1958) The effect of a riboflavin antagonist upon leukocytes of normal and shay myeloid chloroleukemic rats. Blood 13(5):464–474
50. Choi S-K (2004) Synthetic multivalent molecules: concepts and biomedical applications. Wiley, New Jersey
51. Mammen M, Choi SK, Whitesides GM (1998) Polyvalent interactions in biological systems: implications for design and use of multivalent ligands and inhibitors. Angew Chem Int Ed 37:2754–2794
52. Fasting C, Schalley CA, Weber M, Seitz O, Hecht S, Koksch B, Dernedde J, Graf C, Knapp E-W, Haag R (2012) Multivalency as a chemical organization and action principle. Angew Chem Int Ed 51(42):10472–10498
53. Caelen I, Kalman A, Wahlstrom L (2003) Biosensor-based determination of riboflavin in milk samples. Anal Chem 76(1):137–143
54. Wu FYH, MacKenzie RE, McCormick DB (1970) Kinetics and mechanism of oxidation-reduction reactions between pyridine nucleotides and flavins. Biochemistry 9(11):2219–2224
55. Tomalia DA, Naylor AM, Goddard WA (1990) Starburst dendrimers: molecular-level control of size, shape, surface chemistry, topology, and flexibility from atoms to macroscopic matter. Angew Chem Int Ed 29(2):138–175
56. Wong P, Tang S, Mukherjee J, Tang K, Gam K, Isham D, Murat C, Sun R, Baker JR, Choi SK (2016) Light-controlled active release of photocaged ciprofloxacin for lipopolysaccharide-targeted drug delivery using dendrimer conjugates. Chem Commun (Cambridge UK) 52:10357–10360
57. Wong PT, Chen D, Tang S, Yanik S, Payne M, Mukherjee J, Coulter A, Tang K, Tao K, Sun K, Baker JR Jr, Choi SK (2015) Modular integration of upconversion nanocrystal-dendrimer composites for folate receptor-specific near infrared imaging and light triggered drug release. Small 11(45):6078–6090
58. Cloninger MJ (2002) Biological applications of dendrimers. Curr Opin Chem Biol 6(6): 742–748
59. Esfand R, Tomalia DA (2001) Poly(amidoamine) (PAMAM) dendrimers: from biomimicry to drug delivery and biomedical applications. Drug Discov Today 6(8):427–436
60. Majoros I, Baker J Jr (eds) (2008) Dendrimer-based nanomedicine. Pan Stanford, Hackensack
61. Medina SH, El-Sayed MEH (2009) Dendrimers as carriers for delivery of chemotherapeutic agents. Chem Rev (Washington, DC, US) 109(7):3141–3157
62. Rosowsky A, Forsch RA, Wright JE (2004) Synthesis and in vitro antifolate activity of rotationally restricted aminopterin and methotrexate analogues. J Med Chem 47(27): 6958–6963
63. Kiessling LL, Gestwicki JE, Strong LE (2000) Synthetic multivalent ligands in the exploration of cell-surface interactions. Curr Opin Chem Biol 4(6):696–703
64. Horowitz ED, Hud NV (2006) Ethidium and proflavine binding to a 2′,5′-Linked RNA duplex. J Am Chem Soc 128(48):15380–15381
65. Sankaran NB, Nishizawa S, Seino T, Yoshimoto K, Teramae N (2006) Abasic-site-containing oligodeoxynucleotides as aptamers for riboflavin. Angew Chem Int Ed 45(10): 1563–1568
66. Luo D, Saltzman WM (2000) Synthetic DNA delivery systems. Nat Biotechnol 18(1):33–37

67. Herd H, Daum N, Jones AT, Huwer H, Ghandehari H, Lehr C-M (2013) Nanoparticle geometry and surface orientation influence mode of cellular uptake. ACS Nano 7(3):1961–1973
68. Giljohann DA, Seferos DS, Daniel WL, Massich MD, Patel PC, Mirkin CA (2010) Gold nanoparticles for biology and medicine. Angew Chem Int Ed 49(19):3280–3294
69. Daniel M-C, Astruc D (2004) Gold nanoparticles; assembly, supramolecular chemistry, quantum-size-related properties, and applications toward biology, catalysis, and nanotechnology. Chem Rev (Washington, DC, US) 104(1):293–346
70. El-Sayed IH, Huang X, El-Sayed MA (2005) Surface plasmon resonance scattering and absorption of anti-EGFR antibody conjugated gold nanoparticles in cancer diagnostics: applications in oral cancer. Nano Lett 5(5):829–834
71. El-Sayed IH, Huang X, El-Sayed MA (2006) Selective laser photo-thermal therapy of epithelial carcinoma using anti-EGFR antibody conjugated gold nanoparticles. Cancer Lett (NY, NY, US) 239(1):129–135
72. Qian W, Huang X, Kang B, El-Sayed MA (2010) Dark-field light scattering imaging of living cancer cell component from birth through division using bioconjugated gold nanoprobes. J Biomed Opt 15(4):46025–46029
73. Klein S, Petersen S, Taylor U, Barcikowski S, Rath D (2010) Quantitative visualization of colloidal and intracellular gold nanoparticles by confocal microscopy. J Biomed Opt 15(3):36015
74. Lee YC, Lee RT (1995) Carbohydrate-protein interactions: basis of glycobiology. Acc Chem Res 28(8):321–327
75. Choi S-K, Mammen M, Whitesides GM (1997) Generation and in situ evaluation of libraries of poly(acrylic acid) presenting sialosides as side chains as polyvalent inhibitors of influenza-mediated hemagglutination. J Am Chem Soc 119(18):4103–4111
76. Jayaraman N (2009) Multivalent ligand presentation as a central concept to study intricate carbohydrate-protein interactions. Chem Soc Rev 38(12):3463–3483
77. Hong S, Leroueil PR, Majoros IJ, Orr BG, Baker JR Jr, Banaszak Holl MM (2007) The binding avidity of a nanoparticle-based multivalent targeted drug delivery platform. Chem Biol (Oxford UK) 14(1):107–115
78. Li X, Zhou H, Yang L, Du G, Pai-Panandiker AS, Huang X, Yan B (2011) Enhancement of cell recognition in vitro by dual-ligand cancer targeting gold nanoparticles. Biomaterials 32 (10):2540–2545
79. Silpe JE, Sumit M, Thomas TP, Huang B, Kotlyar A, van Dongen MA, Banaszak Holl MM, Orr BG, Choi SK (2013) Avidity modulation of folate-targeted multivalent dendrimers for evaluating biophysical models of cancer targeting nanoparticles. ACS Chem Biol 8(9): 2063–2071
80. Li M-H, Choi SK, Thomas TP, Desai A, Lee K-H, Kotlyar A, Banaszak Holl MM, Baker JR Jr (2012) Dendrimer-based multivalent methotrexates as dual acting nanoconjugates for cancer cell targeting. Eur J Med Chem 47:560–572
81. Thomas TP, Huang B, Choi SK, Silpe JE, Kotlyar A, Desai AM, Gam J, Joice M Jr (2012) Polyvalent PAMAM-methotrexate dendrimer as a folate receptor-targeted therapeutic. Mol Pharm 9(9):2669–2676
82. Thomas TP, Joice M, Sumit M, Silpe JE, Kotlyar A, Bharathi S, Kukowska-Latallo J, Baker JR, Choi SK (2013) Design and in vitro validation of multivalent dendrimer methotrexates as a folate-targeting anticancer therapeutic. Curr Pharm Des 19(37): 6594–6605
83. Wong P, Choi SK (2015) Mechanisms and implications of dual-acting methotrexate in folate-targeted nanotherapeutic delivery. Int J Mol Sci 16(1):1772–1790
84. Choi SK, Myc A, Silpe JE, Sumit M, Wong PT, McCarthy K, Desai AM, Thomas TP, Kotlyar A, Banaszak Holl MM, Orr BG, Baker JR (2013) Dendrimer-based multivalent vancomycin nanoplatform for targeting the drug-resistant bacterial surface. ACS Nano 7(1): 214–228

85. Krishnamurthy VM, Quinton LJ, Estroff LA, Metallo SJ, Isaacs JM, Mizgerd JP, Whitesides GM (2006) Promotion of opsonization by antibodies and phagocytosis of gram-positive bacteria by a bifunctional polyacrylamide. Biomaterials 27(19):3663–3674
86. Qi G, Li L, Yu F, Wang H (2013) Vancomycin-modified mesoporous silica nanoparticles for selective recognition and killing of pathogenic gram-positive bacteria over macrophage-like cells. ACS Appl Mater Interfaces 5(21):10874–10881
87. Kell AJ, Stewart G, Ryan S, Peytavi R, Boissinot M, Huletsky A, Bergeron MG, Simard B (2008) Vancomycin-modified nanoparticles for efficient targeting and preconcentration of gram-positive and gram-negative bacteria. ACS Nano 2(9):1777–1788
88. Li M-H, Choi SK, Leroueil PR, Baker JR (2014) Evaluating binding avidities of populations of heterogeneous multivalent ligand-functionalized nanoparticles. ACS Nano 8(6): 5600–5609
89. Choi S-K, Mammen M, Whitesides GM (1996) Monomeric inhibitors of influenza neuraminidase enhance the hemagglutination inhibition activities of polyacrylamides presenting multiple C-sialoside groups. Chem Biol (Oxford UK) 3:97–104
90. Bhatia S, Dimde M, Haag R (2014) Multivalent glycoconjugates as vaccines and potential drug candidates. MedChemComm 5(7):862–878
91. Zhou H, Jiao P, Yang L, Li X, Yan B (2010) Enhancing cell recognition by scrutinizing cell surfaces with a nanoparticle array. J Am Chem Soc 133(4):680–682
92. Mintzer MA, Dane EL, O'Toole GA, Grinstaff MW (2011) Exploiting dendrimer multivalency to combat emerging and re-emerging infectious diseases. Mol Pharm 9(3): 342–354
93. Bromfield SM, Posocco P, Fermeglia M, Tolosa J, Herreros-López A, Pricl S, Rodríguez-López J, Smith DK (2014) Shape-persistent and adaptive multivalency: rigid transgeden (TGD) and flexible PAMAM dendrimers for heparin binding. Chem Eur J 20(31):9666–9674
94. Bhatia S, Camacho LC, Haag R (2016) Pathogen inhibition by multivalent ligand architectures. J Am Chem Soc 138(28):8654–8666
95. Hlavacek WS, Posner RG, Perelson AS (1999) Steric effects on multivalent ligand-receptor binding: exclusion of ligand sites by bound cell surface receptors. Biophys J 76(6):3031–3043
96. Howard M, Zern BJ, Anselmo AC, Shuvaev VV, Mitragotri S, Muzykantov V (2014) Vascular targeting of nanocarriers: perplexing aspects of the seemingly straightforward paradigm. ACS Nano 8(5):4100–4132
97. Choi SK, Leroueil P, Li M-H, Desai A, Zong H, Van Der Spek AFL, Baker JR Jr (2011) Specificity and negative cooperativity in dendrimer-oxime drug complexation. Macromolecules 44(11):4026–4029
98. Gomez-Casado A, Dam HH, Yilmaz MD, Florea D, Jonkheijm P, Huskens J (2011) Probing multivalent interactions in a synthetic host-guest complex by dynamic force spectroscopy. J Am Chem Soc 133(28):10849–10857
99. Roy R (1996) Syntheses and some applications of chemically defined multivalent glycoconjugates. Curr Opin Struct Biol 6(5):692–702
100. Mullen DG, Fang M, Desai A, Baker JR Jr, Orr BG, Banaszak Holl MM (2010) A quantitative assessment of nanoparticle-ligand distributions: implications for targeted drug and imaging delivery in dendrimer conjugates. ACS Nano 4(2):657–670
101. Teulon J-M, Delcuze Y, Odorico M, S-wW Chen, Parot P, Pellequer J-L (2011) Single and multiple bonds in (strept)avidin-biotin interactions. J Mol Recognit 24(3):490–502